arXiv:1407.5851v1 [astro-ph.SR] 22 Jul 2014

Parametric decay of parallel and oblique Alfvén waves in the expanding solar wind

L. Del Zanna[1,2,3]†, L. Matteini[1,4], S. Landi[1,2], A. Verdini[1,5], M. Velli[1,6]

[1]Dipartimento di Fisica e Astronomia, Università degli Studi di Firenze, Italy
[2]INAF - Osservatorio Astrofisico di Arcetri, Firenze, Italy
[3]INFN - Sezione di Firenze, Italy
[4]Space and Atmospheric Physics Group, Imperial College London, UK
[5]Solar–Terrestrial Center of Excellence, Royal Observatory of Belgium, Brussels, Belgium
[6]Jet Propulsion Laboratory, California Institute of Technology, Pasadena, California, USA

(Received ?; revised ?; accepted ?. - To be entered by editorial office)

The long-term evolution of large-amplitude Alfvén waves propagating in the solar wind is investigated by performing two-dimensional MHD simulations within the expanding box model. The linear and nonlinear phases of the parametric decay instability are studied for both circularly polarized waves in parallel propagation and for arc-polarized waves in oblique propagation. The non-monochromatic case is also considered. In the oblique case, the direct excitation of daughter modes transverse to the local background field is found for the first time in an expanding environment, and this transverse cascade seems to be favored for monochromatic mother waves. The expansion effect reduces the instability growth rate, and it can even suppress its onset for the lowest frequency modes considered here, possibly explaining the persistence of these outgoing waves in the solar wind.

PACS codes: To be inserted later.

1. Introduction

An exceptional laboratory for plasma physics and magnetohydrodynamics (MHD) is represented by the solar wind, the supersonic continuous outflow originating from the hot ($T > 10^6 K$) corona of the Sun and permeating the whole heliosphere. The low-frequency part of fluctuations spectrum ($\nu \sim 10^{-4} - 10^{-2}$ Hz) in high-speed and polar regions of the solar wind is known to be dominated by large-amplitude Alfvén waves propagating outwards (Belcher & Davis 1971; Bruno *et al.* 1985; Roberts *et al.* 1987; Grappin *et al.* 1990; Marsch & Tu 1990; Tu & Marsch 1990; Goldstein *et al.* 1995; Horbury *et al.* 2005). The presence of such waves is also seen to affect the correlation between the wind speed itself and the local field direction (Matteini *et al.* 2014). The ratio of incoming to outgoing wave energies gradually increases and saturates at heliocentric distances of about 2.5 AU (Bavassano *et al.* 2000; Bruno & Carbone 2013), as derived from data from the *Ulysses* spacecraft, which has probed the mostly uniform polar wind. This behavior appears to contradict the so-called *dynamical alignment* (Dobrowolny *et al.* 1980), for which any initial imbalance in the Alfvénic modes should actually be reinforced by the nonlinear interactions, at least within the framework of incompressible MHD.

However, in the solar wind plasma, compressibility effects are certainly likely to be influent. An important consequence is that an Alfvén wave propagating on a background

† luca.delzanna@unifi.it

magnetic field while preserving its (even large) amplitude, in spite of being an exact solution of the full MHD equations, after some time becomes unstable because of wave-wave coupling with compressible modes and decays into a backscattered Alfvénic mode and a forward propagating acoustic mode (Galeev & Oraevskii 1963; Sagdeev & Galeev 1969), which are resonantly amplified. Thus, compressible modes are not only important for their natural tendency to steepening, shock dissipation, and subsequent plasma heating, but also they may be responsible for the simultaneous presence of opposite propagating Alfvénic modes, which is a necessary condition for the development of (incompressible) MHD turbulence.

Such *parametric decay instability* is generally stronger in a low-beta plasma and for large amplitudes of the pump (or mother) Alfvén wave. Analytical results are concerned with the complete dispersion relation (Derby 1978; Goldstein 1978) and some limiting regimes (Hollweg 1994). Numerical MHD simulations investigated various aspects of this instability, from the dependence on the plasma beta, to the propagation in multi-dimensions, to the different polarizations, to the presence of an initial broad-band spectrum of fluctuations (Hoshino & Goldstein 1989; Viñas & Goldstein 1991; Umeki & Terasawa 1992; Ghosh *et al.* 1993; Malara & Velli 1996; Malara *et al.* 2000; Del Zanna *et al.* 2001; Del Zanna 2001). In these latter papers it was shown that parametric decay can indeed be responsible for the observed gradual increase of incoming Alfvénic flux with distance, or correspondingly the reduction of the normalized *cross helicity* σ_c (see Inhester 1990, for a critical discussion), whereas its saturation at a certain distance can be easily explained by the natural suppression of the decay instability itself when the nonlinear regime is reached.

In particular, Del Zanna *et al.* (2001) showed that the saturation of the instability always occurs when the daughter acoustic mode has steepened into a train of quasi-parallel shocks, that may eventually contribute to the plasma heating. This may be important in solar coronal holes, where the plasma beta is lower and the decay more efficient (decay time and length-scales are shorter and up to half of the initial Alfvénic energy is observed to go into heat), and where the lack of large-scale magnetic structures suggests to exclude other mechanisms (Del Zanna & Velli 2002). However, even at larger heliocentric distances, where the beta is higher and also the fluid description should break down in favor of a kinetic regime, hybrid simulations of parametric instabilities show plasma heating via particle trapping in the potential wells associated with the steepened resonant density perturbation (Nariyuki & Hada 2006; Nariyuki *et al.* 2007; Araneda *et al.* 2008; Matteini *et al.* 2010*a*,*b*). Moreover, proton velocity beams are seen to develop in the distribution functions, reminiscent of what is observed in real data.

Another important issue is that the majority of the observed large-amplitude Alfvén waves in the solar wind are found with a spherical *arc-like* polarization (Riley *et al.* 1996; Tsurutani & Ho 1999). This means that one should not restrict the analysis to circularly polarized waves in parallel propagation, with respect to the average background magnetic field, but it is important to study the more general case of oblique propagation. Numerical investigations (Vasquez & Hollweg 1996; Del Zanna 2001) have shown that the basic properties of the instability are preserved, and that in addition this can also lead to a *direct* creation of transverse small-scales (Matteini *et al.* 2010*a*; Del Zanna *et al.* 2012*b*). This possibility may provide a complementary mechanism to (or at least a seed for) strong Alfvénic turbulence (Breech *et al.* 2005). Notice that the simultaneous presence of compressible heating and transverse Alfvénic turbulence appears to be required in stationary models for fast solar wind acceleration (Verdini & Velli 2007; Verdini *et al.* 2010). See however Lionello *et al.* (2014) for a comparison with a time-dependent model.

In order to properly study the nonlinear wave or turbulence evolution in the solar

wind, the effects of the radial expansion should be taken into account. Cartesian-like periodic domains are usually employed for such kind of simulations, here we adopt the so-called *expanding box* (EB) model (Velli *et al.* 1992; Grappin *et al.* 1993; Grappin & Velli 1996), also adapted to kinetic and hybrid models (Liewer *et al.* 2001; Hellinger *et al.* 2005; Matteini *et al.* 2006). The radial expansion effects are mimicked by introducing a lateral stretching of a local frame comoving with the solar wind velocity. In this model, effects like the gradual decrease in wave amplitude and the development of the Parker spiral are easily recovered.

The EB model has been recently implemented in the *Eulerian Conservative High Order* (`ECHO`) code for classical and relativistic MHD (Del Zanna *et al.* 2007; Landi *et al.* 2008; Del Zanna 2009), taking advantage of the freedom in the choice of the spatial metric. Preliminary test simulations (Del Zanna *et al.* 2012*a*) have shown that the expansion is likely to affect the instability growth and even to prevent it, depending on the respective characteristic time-scales. A one-dimensional investigation of the effects of a non-uniform wind velocity on parametric decay has also been recently performed by Tenerani & Velli (2013). This should be appropriate for coronal holes and for the wind accelerating region where the flow may still be sub-Alfvénic.

In the present paper we perform two-dimensional MHD simulations by applying the EB model to circularly polarized Alfvén waves in parallel propagation, and to arc-polarized Alfvén waves in oblique propagation, to study the direct excitation of perpendicular modes. Both monochromatic mother waves or an initial broad-band spectrum will be considered. The effect of the solar wind expansion will be investigated by changing the location of the initial position of the comoving box. The paper is organized as follows. The EB-MHD equations and their implementation in the `ECHO` code are described in Sect. 2, the initial conditions and setup relevant for the simulations of parametric decay are in Sect. 3, simulation results will be shown in Sect. 4, while conclusions will be given in Sect. 5.

2. The Expanding Box model for MHD

When studying numerically wave motion or any kind of plasma instabilities, it is more convenient, whenever possible, to use a local simulation box in Cartesian-like coordinates and periodic boundary conditions. Within such settings the physical effect under investigation can be more easily singled out and high-accuracy numerical methods employed. In the present section we first describe the original version of the EB model, leading to a few additional source terms in the set of MHD equations, and a novel one, more appropriate for multi-purpose conservative schemes working in any system of coordinates.

In the case of the solar wind, it is useful to consider a parcel of plasma in the radially expanding outflow, characterized by a given background velocity profile $U(R)$. If we identify the heliocentric distance of the parcel in time with $R(t)$, so that $dR/dt \equiv U(R)$, it is convenient to introduce, in analogy with cosmology, the *expansion scale factor*

$$a(t) = \frac{R(t)}{R_0}, \quad \frac{\dot{a}}{a} = \frac{U(R)}{R}, \tag{2.1}$$

where $R_0 \equiv R(0)$ is the initial parcel position, the dot indicates time derivation, and the latter quantity in Eq. (2.1) is the inverse of the expansion characteristic time, basically the analog of the cosmological Hubble time.

Let us now choose a locally Cartesian-like coordinate system with $x = r - R(t)$ and *stretched* transverse coordinates y and z, expanding precisely at the rate $a(t)$ due to the radially diverging geometry. Provided the box is taken sufficiently small such that the

wind speed can be considered as uniform, the latter can be removed with a Galilean transformation. In the new *comoving* frame $x^1 = x$, $x^2 = y/a$, $x^3 = z/a$ the residual velocity is, to first-order expansion

$$\mathbf{u}_\perp = \dot{a}\,(0, x^2, x^3) = (\dot{a}/a)(0, y, z), \tag{2.2}$$

clearly non-vanishing in the transverse direction. In the evolution equations, time derivatives and (transverse) spatial gradients are therefore modified as

$$\partial_t \;\to \partial_t - (\mathbf{u}_\perp \cdot \nabla), \quad \nabla = (\partial_1,\, a^{-1}\partial_2,\, a^{-1}\partial_3) = (\partial_x, \partial_y, \partial_z), \tag{2.3}$$

so that novel source terms are expected to appear.

The system of ideal MHD equations in the EB approximation is (Grappin *et al.* 1993):

$$\partial_t \rho + \nabla \cdot (\rho \mathbf{v}) = -(\dot{a}/a) 2\rho, \tag{2.4}$$

$$\rho(\partial_t + \mathbf{v}\cdot\nabla)\mathbf{v} - (\mathbf{B}\cdot\nabla)\mathbf{B} + \nabla(p + B^2/2) = -(\dot{a}/a)\rho\mathbf{v}\cdot\mathcal{T}, \tag{2.5}$$

$$(\partial_t + \mathbf{v}\cdot\nabla)p + \Gamma p \nabla\cdot\mathbf{v} = -(\dot{a}/a) 2\Gamma p, \tag{2.6}$$

$$\partial_t \mathbf{B} - \nabla\times(\mathbf{v}\times\mathbf{B}) = -(\dot{a}/a)\mathbf{B}\cdot(2\mathcal{I} - \mathcal{T}). \tag{2.7}$$

In the above equations ρ is the density, $\mathbf{v}$ is the velocity in the comoving frame, p is the thermal pressure, $\mathbf{B}$ is the magnetic field (we use Gaussian units with $4\pi \to 1$), $\mathcal{I}$ is the identity tensor, $\mathcal{T} = \mathrm{diag}\{0, 1, 1\}$, and $\Gamma = 5/3$ is the adiabatic index for an ideal monoatomic gas.

The above ideal EB-MHD equations predict, even for a static and uniform plasma, an evolution $\rho \sim a^{-2}$, $T \sim p/\rho \sim a^{-2(\Gamma-1)} \sim a^{-4/3}$, $B_x \sim a^{-2}$, $B_y \sim a^{-1}$, $B_z \sim a^{-1}$, just due to the lateral stretching (notice the formation of the Parker spiral, in the $x-y$ plane, as $\tan\theta = B_y/B_x \sim a$). If Alfvénic fluctuations are present, in the strong coupling regime the WKB approximation for small amplitudes and short wavelengths predicts that $\delta v^2 \sim \delta B^2/\rho \sim a^{-1}$. The model of the expanding box is thus able to capture all known scaling laws with heliocentric distance.

In order to study numerically the nonlinear evolution of Alfvén waves, it is convenient to adopt the conservative formulation for the MHD equations. In particular, the `ECHO` code solves for the classical (and relativistic) MHD equations in the general form

$$\partial_t \mathcal{U} + \partial_i \mathcal{F}^i = \mathcal{S}, \tag{2.8}$$

where $\mathcal{U}$ is a generic vector of conservative variables, $\mathcal{F}^i$ are the corresponding fluxes (latin indexes like i run on the 3 spatial coordinates x^i and the Einstein convention of a sum over repeated indexes is implicitly assumed), and $\mathcal{S}$ is the vector containing the source terms. Given a generic spatial metric tensor g_{ij}, with determinant g, the MHD system is retrieved by choosing

$$\mathcal{U} = \sqrt{g}\begin{bmatrix} \rho \\ \rho v_j \\ E_t \\ B^j \end{bmatrix}, \quad \mathcal{F}^i = \sqrt{g}\begin{bmatrix} \rho v^i \\ \rho v^i v_j - B^i B_j + p_t \delta^i_j \\ (E_t + p_t)v^i - (v_k B^k) B^i \\ v^i B^j - v^j B^i \end{bmatrix}, \tag{2.9}$$

where the *total* kinetic plus magnetic pressure and energy are

$$p_{\rm t} = p + \tfrac{1}{2}B^2, \quad E_{\rm t} = \tfrac{1}{2}\rho v^2 + \tfrac{1}{\Gamma-1}\,p + \tfrac{1}{2}B^2, \tag{2.10}$$

and the source terms are

$$\mathcal{S} = \sqrt{g} \begin{bmatrix} 0 \\ \frac{1}{2}(\rho v^i v^k - B^i B^k + p_t g^{ik})\partial_j g_{ik} \\ -\frac{1}{2}(\rho v^i v^j - B^i B^j + p_t g^{ij})\partial_t g_{ij} \\ 0 \end{bmatrix}. \tag{2.11}$$

Obviously, for non-Cartesian metrics, care must be taken to the differences between covariant and contravariant components (related by $v_i = g_{ij}v^j$).

It is now straightforward to introduce EB within such framework. Given the scale factor $a = a(t)$ of Eq. 2.1 yielding the transverse expansion, the metric tensor must be necessarily defined as

$$g_{ij} = \mathrm{diag}\{1, a^2(t), a^2(t)\}, \quad \sqrt{g} = a^2(t), \tag{2.12}$$

thus the metric is almost Cartesian (diagonal and spatially uniform), but time-dependent. If we want to employ the usual Cartesian orthonormal x, y, and z components, we must recall that for a generic vector v^i we have $v_1 = v^1 = v_x$, $v_2 = a^2 v^2 = a v_y$, $v_3 = a^2 v^3 = a v_z$. Notice that the source term in the momentum equation vanishes ($\partial_j g_{ik} = 0$), while that in the energy equation is given by

$$-\tfrac{1}{2}(\rho v^i v^j - B^i B^j + p_t g^{ij})\partial_t g_{ij} = -\frac{\dot{a}}{a}(\rho v_\perp^2 - B_\perp^2 + 2p_t), \tag{2.13}$$

where $v_\perp^2 = v_y^2 + v_z^2$ and similarly for the magnetic field. The original non-conservative EB-MHD equations described previously are equivalent to the form above required by the `ECHO` code, as it can be easily verified (recall that $\partial_1 = \partial_x$, $\partial_2 = a\partial_y$, $\partial_3 = a\partial_z$).

In the present paper we will only consider the evolution of Alfvén waves at large heliocentric distances, where the outflow is super-Alfvénic and $U(R)$ can be considered as constant. For an investigation appropriate to the solar wind acceleration region see Tenerani & Velli (2013), where the relevant modifications to the equations can also be found. Here we thus choose for simplicity $U(R) \equiv U_0$ and

$$R(t) = R_0 + U_0 t, \quad a(t) = 1 + \epsilon t, \quad \frac{\dot{a}}{a} = \frac{\epsilon}{1+\epsilon t}, \tag{2.14}$$

where $\epsilon \equiv U_0/R_0$ is the *constant* expansion rate, or, equivalently, the inverse of the characteristic expansion time.

3. Simulation setup

The quantities appearing in the MHD equations previously described, and in the initial conditions of the present section, are normalized against values at the reference distance $R_0 \equiv R(0)$ at simulation time $t = 0$. We choose Alfvénic units throughout the paper: a density ρ_0, a background magnetic field with strength B_0, a basic wave period τ_A, so that the Alfvén speed is $v_\mathrm{A} = B_0/\sqrt{\rho_0}$, and any length will be expressed in terms of the basic wavelength $\lambda_\mathrm{A} = v_\mathrm{A}\tau_\mathrm{A}$. At the initial position R_0 and time $t = 0$ we also define the plasma beta $\beta = c_\mathrm{s}^2/v_\mathrm{A}^2$, where $c_\mathrm{s}^2 = \Gamma p_0/\rho_0$ is the square of the sound speed.

The initial conditions are provided as follows. Once the values of the plasma beta β and of the normalized mother wave amplitude η have been chosen, we set up an unperturbed static plasma with density $\rho = 1$, pressure $p = \beta/\Gamma$, velocity $\mathbf{v} = 0$, background field

$$\mathbf{B}_0 = \cos\theta_0 \mathbf{e}_x + \sin\theta_0 \mathbf{e}_y, \tag{3.1}$$

where θ_0 is the initial angle of the Parker spiral at R_0, and Alfvénic fluctuations

$$\delta\mathbf{B} = \eta\cos(\varphi)\mathbf{e}_z + \mathcal{F}(\varphi)\mathbf{e}_y, \quad \delta\mathbf{v} = -\delta\mathbf{B}, \tag{3.2}$$

where $\varphi = \mathbf{k}_0\cdot\mathbf{x} \equiv k_0 x$ is the phase for the *monochromatic* case (see however Sect. 4.3), $\mathbf{k}_0 = k_0\mathbf{e}_x$, with $k_0 = 2\pi$, is the wave vector of the pump (mother) wave.

The function $\mathcal{F}$ is derived by the condition $|\mathbf{B}_0 + \delta\mathbf{B}| = \text{const}$ and depends on the chosen polarization, as described below.

• *Circular polarization (parallel propagation)* – the oscillations are always orthogonal to both $\mathbf{k}_0$ and $\mathbf{B}_0$, taken to be radial with $\theta_0 = 0$, and

$$\mathcal{F}(\varphi) = \eta\sin(\varphi); \tag{3.3}$$

• *Arc polarization (oblique propagation)* – in this case $\mathbf{k}_0$ and $\mathbf{B}_0$ are not parallel and B_y has both a background and an oscillating part. By imposing $C^2 = B_y^2 + B_z^2 = B^2 - {B_0}_x^2$ and $<\delta B_y>= 0$ (Barnes & Hollweg 1974; Del Zanna 2001) we find

$$\mathcal{F}(\varphi) = \sqrt{C^2 - \eta^2\cos^2(\varphi)} - \sin\theta_0, \tag{3.4}$$

where the unknown constant C is derived by solving the elliptic integral

$$\frac{2}{\pi}\int_0^{\pi/2}\sqrt{C^2 - \eta^2\cos^2\varphi}\,\mathrm{d}\varphi = \sin\theta_0, \tag{3.5}$$

which admits solutions only if $\sin\theta_0 > 2\eta/\pi$.

The pump Alfvén waves in either circular or arc polarization described above are *exact* solutions of the ideal MHD equations (without expansion), and propagate with

$$\omega_0 = \mathbf{k}_0\cdot\mathbf{v}_\mathrm{A} = k_0\cos\theta_0, \tag{3.6}$$

preserving $B = |\mathbf{B}_0 + \delta\mathbf{B}|$ and $|\delta\mathbf{v}|$, even if the amplitude η is large, constant in time during the evolution. A last possibility is of course to abandon the condition of a constant B for a simpler *linear* polarization with $\mathcal{F}(\varphi) = 0$, either in parallel ($\theta_0 = 0$) or oblique propagation, but the evolution is affected by ponderomotive pressure forces proportional to η^2, and will not be considered here.

Parametric decay occurs when compressibility is taken into account. Small-scale density perturbations may grow resonantly due to three-modes wave-wave nonlinear interactions and the energy of the pump wave is partially transferred to two daughter waves. For quasi-normal modes (small amplitudes), and in the low-beta regime, the mother wave ($\omega_0 = k_0$) decays into a forward propagating sound wave ($\omega_c = \sqrt{\beta}k_c$) and a back-scattered Alfvén wave ($\omega^- = k^-$), where parallel propagation has been considered for simplicity. Under these approximations, the resonance condition is found by the scattering relations $\omega_0 = \omega_c + \omega^-$ and $k_0 = k_c - k^-$, leading to $k_c/k_0 = 2/(1+\sqrt{\beta})$ and $k^-/k_0 = (1-\sqrt{\beta})/(1+\sqrt{\beta})$. The growth rate of the instability can be approximated as (Galeev & Oraevskii 1963) $\gamma/\omega_0 \simeq \eta\beta^{-1/4}/2$, so it is stronger for a low-beta plasma and for large amplitudes. For generic values of η and β, that is even for large amplitudes and warm plasmas, one needs to solve the full dispersion relation. For circularly polarized waves and parallel propagation it reads (Derby 1978; Goldstein 1978):

$$(\omega - k)(\omega^2 - \beta k^2)[(\omega + k)^2 - 4] = \eta^2 k^2(\omega^3 + k\omega^2 - 3\omega + k), \tag{3.7}$$

where $k/k_0 \to k$ and $\omega/\omega_0 \to \omega$, looking for the range of unstable modes. For instance, if we consider $\eta = 0.2$ and $\beta = 0.1$, the resulting maximum growth rate is $\gamma/\omega_0 \simeq 0.11$, obtained for the compressive mode with wave number $k_c/k_0 \simeq 1.55$. In the oblique case, if retaining the 1D approximation $\mathbf{k}_0 = k_0\mathbf{e}_x$, these numbers scale as $\cos\theta_0$, since $\omega_0 = k_0\cos\theta_0$, though the parallel case can not be retrieved for $\theta_0 = 0$ (Del Zanna 2001).

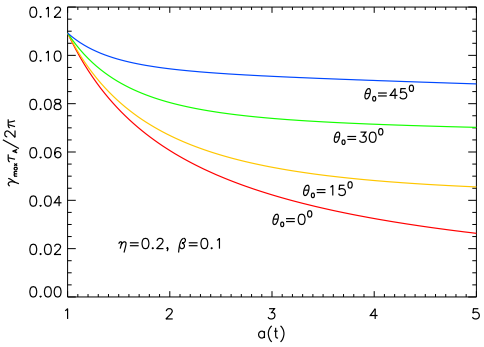

FIGURE 1. The maximum growth rate for the decay instability as a function of the expansion scale factor $a = R(t)/R_0$, for $\eta = 0.2$, $\beta = 0.1$, and circular polarization. Different values of the initial angle θ_0 in the equatorial plane are compared.

However, during the evolution in the expanding solar wind plasma the parameters ω_0, η, and β are all dependent on R and thus also time-dependent with $a(t)$. For parallel propagation we have $\omega_0 \sim a^{-1}$, $\eta \sim a^{1/2}$, and $\beta \sim a^{2/3}$, so that the growth rate is expected to decrease in time as $\gamma \sim a^{-2/3}$ (Tenerani & Velli 2013). On the other hand, if the development of the Parker spiral is taken into account, that is when $\theta_0 > 0$, the magnitude of the background field should decrease initially as $B \sim a^{-2}$ (when B_x is dominant) and after a certain radius as $B \sim a^{-1}$ (when B_y is dominant), so that ω_0 becomes constant while $\eta \sim a^{-1/2}$ and $\beta \sim a^{-1/3}$ start to decrease with time (and distance). The growth rate of the parametric instability is now expected to decrease as $\gamma \sim a^{-5/12}$. The above estimates are valid when the expansion rate is small compared to the growth rate, and for small values of η and β. For the most general case of warm plasmas and large amplitudes, still preserving the condition $\epsilon \ll \gamma$, one has instead to solve Eq. 3.7 with input values rescaled by the expansion factor. Results are plotted in Fig. 1, where the maximum rate as a function of $a(t)$ is plotted for different values of θ_0.

Simulations will be performed in the ecliptic plane $x - y$ by using a two-dimensional numerical domain $[0, L_x] \times [0, L_y]$, where $L_x = L_y = m_0 \lambda_A$ at the initial time, and $L_y \sim a$ will be stretched due to solar wind radial expansion, as a built-in effect characteristic of EB. Notice that, due to expansion, not only the maximum growth rates diminish but also the correspondent wave numbers. Thus, m_0 must be sufficiently high in order to have room for daughter waves to fully develop in our numerical domain with periodical boundary conditions, especially in the oblique case where transverse modes are expected to be excited too. We choose throughout the paper the value $m_0 = 10$.

Finally, we must choose reference values for our parameters and ensure that the EB approximation is applicable. The normalized expansion parameter is

$$\epsilon = 5.0 \times 10^{-2} \left(\frac{U_0}{750 \text{ km s}^{-1}} \right) \left(\frac{R_0}{1 \text{ AU}} \right)^{-1} \left(\frac{\tau_A}{10^4 \text{ s}} \right), \tag{3.8}$$

increasing for smaller values of the initial radial distance of the box R_0. We choose $R_0 = 0.25$ AU, so that the evolution will be limited in the range where *in situ* data are available, from the Helios mission in the inner region up to the Earth's orbit and beyond. For fast streams in the ecliptic plane at that distance we assume the wind velocity to be already in its asymptotic regime with $U_0 = 750$ km s^{-1}. If $\tau_A = 10^4$ s we find the maximum expansion rate of $\epsilon = 0.2$. Moreover, assuming a dependence of $\propto 1/r$ for the Alfvén speed (we use the value $v_A = 50$ km s^{-1} at 1 AU), we are able to estimate the

TABLE 1. List of simulation parameters

Run	ϵ	θ_0	η	β	k_0	m_0	$m_{c\parallel}$	$m_\parallel^-$	γ
`A0-Par`	0.000	0°	0.2	0.1	2π	10	15	5	0.63
`A1-Par`	0.002	0°	0.2	0.1	2π	10	15	5	0.62
`A2-Par`	0.020	0°	0.2	0.1	2π	10	15	5	0.51
`A3-Par`	0.200	0°	0.2	0.1	2π	10	15	5	–
`A0-Obl`	0.000	30°	0.2	0.1	2π	10	16	6	0.39
`A1-Obl`	0.002	30°	0.2	0.1	2π	10	16	6	0.38
`A2-Obl`	0.020	30°	0.2	0.1	2π	10	16	6	0.27
`A3-Obl`	0.200	30°	0.2	0.1	2π	10	16	6	–
`Nonmon`	0.020	30°	0.2	0.1	2π	10	15	5	0.22

maximum length for the numerical box, which must satisfy the rule

$$\frac{L_x/m_0}{R_0} \ll 3.3\times 10^{-3}\left(\frac{v_\mathrm{A}}{50\ \mathrm{km\ s^{-1}}}\right)\left(\frac{R_0}{1\ \mathrm{AU}}\right)^{-2}\left(\frac{\tau_\mathrm{A}}{10^4\ \mathrm{s}}\right), \tag{3.9}$$

that is the Alfvén wavelength $\lambda_\mathrm{A} = v_\mathrm{A}\tau_\mathrm{A}$ (m_0 modes in the box of length L_x) must be smaller than the scale of the background gradients, of the order of R_0.

When $R_0 = 0.25$ AU and $m_0 = 10$ we see that $L_x \approx 0.5R_0$, so that the maximum period that we are able to study is indeed $\tau_\mathrm{A} = 10^4$ s, whereas higher frequencies would be much better suited. In our simulations we will investigate the Alfvénic period $\nu_\mathrm{A} = 10^{-4} - 10^{-2}$ Hz, as observed at Helios distances, corresponding to an *injection* spectrum ν^{-1} of modes, presumably still of solar origin, that we will use as pump waves for the decay instability.

4. Results

Simulations are performed by employing the `ECHO` code for classical, ideal MHD where the EB has been implemented as described in Sect. 2. We use 512×512 grid points and high-order finite-difference methods, namely a fifth order MPE5 upwind spatial reconstruction (Del Zanna *et al.* 2007; Landi *et al.* 2008) and third order Runge-Kutta time integration, with a Courant number of 0.5. The solenoidal constraint for the magnetic field is enforced through the Upwind Constrained Transport (UCT) method (Londrillo & Del Zanna 2004). All simulations are initialized by adding a white noise of 10^{-4} density random fluctuations in order to trigger the instability.

Run A parameters, namely $\eta = 0.2$ and $\beta = 0.1$ (Del Zanna *et al.* 2001; Del Zanna 2001), will be chosen as default values, whereas different values of the expansion rate ϵ will be selected by choosing the pump wave period τ_A. Both the parallel (circular polarization) and oblique (arc polarization) cases will be studied. A last run will be devoted to a non-monochromatic (oblique) case. The list of parameters for each run is listed in Table 1.

Let us mention that runs with different sets of parameters have also been performed, in particular Run B ($\eta = 0.5$, $\beta = 0.5$) and Run C ($\eta = 1$, $\beta = 1.2$) in the cited papers. These values were selected in order to obtain similar growth rates for the decay instability and to mimic different conditions of the solar wind plasma, namely those for an increasing heliocentric distance (here included in the EB approach). Results are

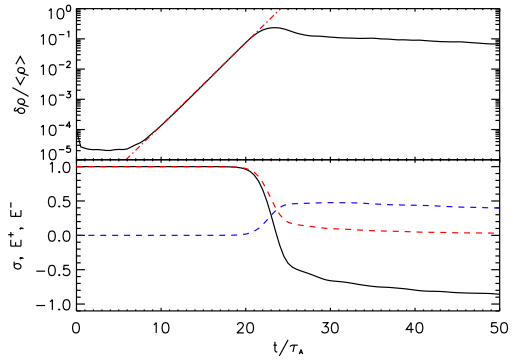

FIGURE 2. Results from a simulation of parallel propagating Alfvén waves and no expansion ($\epsilon = 0$, run `A0-Par`). The instability grows with a measured rate $\gamma = 0.63$ (the dot-dashed fit line). In the top panel we show the *rms* density fluctuations as a function of time, whereas in the bottom panel we plot the corresponding cross helicity and the Elsässer energies (dashed lines).

qualitatively similar, therefore we prefer not to show all of them here. We would just like to remind that Run C parameters are those more suitable to explain the observed saturation of the cross helicity to $\sigma \simeq 0.3$ at ~ 2.5 AU (Bavassano *et al.* 2000). As previously showed (Del Zanna *et al.* 2012*a*), even 1D runs in parallel propagation, with an expansion rate $\epsilon = 0.05$, seems adequate to reproduce the data.

4.1. *Parallel propagation of circularly polarized Alfvén waves*

Before presenting the effects of the solar wind expansion, we first show an introductory run with $\epsilon = 0$, to explain the basics of parametric decay and define some important characteristic quantities. Thus we start by studying the evolution of a parallel propagating pump Alfvén wave with $\theta_0 = 0$ and circular polarization (run `A0-Par`).

In Fig. 2 we can follow the main indicators for the decay instability. In the above panel we show the root mean square (*rms*) density fluctuations, in logarithmic scale, as function of the time t. The linear phase of the decay instability is clearly evident, and an estimation of the exponential growth of density fluctuations yields $\gamma = 0.63$, close to the expected value of $\gamma = 0.11 \times 2\pi = 0.69$ for the *maximum* growth rate predicted by Eq. 3.7. This 10% error is partly due to the fact that in a periodic domain it is almost impossible to retrieve the most unstable mode, since only integer numbers of wavelengths are allowed, thus only selected wave numbers can be retrieved. Moreover, *rms* quantities refer to a mixture of unstable modes, in our case $m_c = 15$ and $m_c = 16$ (a spectral analysis would be required to single out the different modes), and even in parallel propagation 2D effects may play a role (excitation of transverse modes, see below). A fit to a 1D run, preserving the same resolution of 512 grid points, leads to a slightly larger rate $\gamma = 0.64$, to be compared with the theoretical expectations from Eq. 3.7 of $\gamma(m_c = 15) = 0.65$ and $\gamma(m_c = 16) = 0.66$ (we recall that the peak would be for $m_c \simeq 15.5$), corresponding to errors of $1.5 - 3\%$, respectively.

Additional diagnostics comes from the time dependency of Elsässer energies. In the bottom panel of Fig. 2 we plot

$$E^{\pm} =< \tfrac{1}{2}|\mathbf{z}^{\pm}|^2 >, \quad \mathbf{z}^{\pm} = \delta\mathbf{v} \mp \delta\mathbf{B}/\sqrt{\rho}, \tag{4.1}$$

normalized against the initial E^+ value, together with the cross helicity

$$\sigma = \frac{E^+ - E^-}{E^+ + E^-}, \tag{4.2}$$

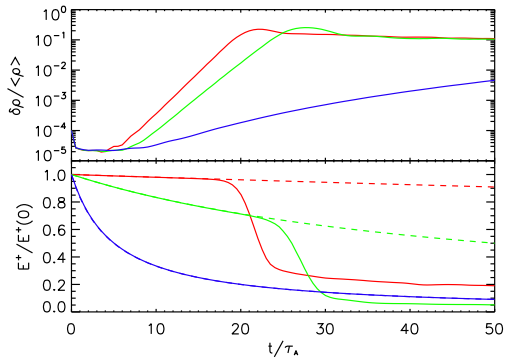

FIGURE 3. Comparison of three simulations with mother wave in parallel propagation. Curves from top to bottom: $\epsilon = 0.002$ (`A1-Par`, red lines in the color version), $\epsilon = 0.02$ (`A2-Par`, green), and $\epsilon = 0.2$ (`A3-Par`, blue). In the top panel density fluctuations are shown as a function of time, whereas in the bottom panel we plot the normalized energy associated to $\mathbf{z}^+$, compared with the expected $E^+ \sim [a(t)]^{-1}$ evolution in the absence of instability (dashed curves).

whose value is $\sigma = +1$ until the pump wave dominates and starts to decrease when the instability peaks, around $t = 20$ in this case. When the compressive mode at $k_c > k_0$ has fully developed, shock heating is known to take place, the instability saturates and density fluctuations cease to increase. Correspondingly, the E^+ energy decreases and the Alfvénic backscattered mode gains energy. This process is strongly dependent on the value of the plasma β. In such a low-β case we find that σ even approaches -1, meaning that $E^+ \to 0$ and an almost pure new pump wave $\mathbf{z}^-$ (with $k^- < k_0$) is present. As previously noticed, this situation leads to multiple decays at longer times (Del Zanna *et al.* 2001).

We start our analysis of the effects of the expansion by investigating the case of parallel propagation ($\mathbf{k}_0 \parallel \mathbf{B}_0 \Rightarrow \theta_0 = 0$) and circular polarization of the pump Alfvén wave. As for the test case without expansion, we employ the usual parameters ($\eta = 0.2$, $\beta = 0.1$) and the numerical settings previously described. As far as expansion is concerned, we run here three simulations with $\epsilon = 0.002$ (`A1-Par`), $\epsilon = 0.02$ (`A2-Par`), and $\epsilon = 0.2$ (`A3-Par`). If we choose a constant wind speed $U_0 = 750$ km s^{-1} and an initial position $R_0 = 0.25$ AU, then the three values span the whole Alfvénic range for frequencies from $\nu_A = 10^{-2}$ Hz ($\epsilon = 0.002$) to $\nu_A = 10^{-4}$ Hz ($\epsilon = 0.2$), according to Eq. 3.8.

The chosen values of ϵ must be compared with the expected instability growth rate $\gamma = 0.63$ for the parameters already employed for `A0-Par` in the absence of expansion. Since $\epsilon = U_0/R_0 = \dot{a}/a(0)$, when this *Hubble-like* term satisfy $\epsilon \ll \gamma$ only minor effects are expected on the exponential growth of the instability, but when $\epsilon \lesssim \gamma$ the instability is strongly modified or even suppressed (Del Zanna *et al.* 2012*a*), and if still present the growth in time becomes algebraic rather than exponential (Tenerani & Velli 2013). This is not surprising: in the first case the pump wave can still be seen as a quasi-stationary solution of the unperturbed problem, while for $\epsilon \lesssim \gamma$ it becomes a time-dependent solution, and the growth can not be any longer exponential. The first two cases corresponding to $\nu_A = 10^{-2}$ Hz and $\nu_A = 10^{-3}$ Hz belong to the first category, while pump waves at the lowest frequency limit of the observed Alfvénic range, namely $\nu_A = 10^{-4}$ Hz ($\epsilon = 0.2$), are expected to have non-exponentially growing daughter modes.

In Fig. 3 we show the comparison of the quantities characterizing the evolution of the decay instability for the three runs. In the top panel we plot the density *rms* fluctuations (normalized to the local average density at every time), it is evident that for $\epsilon = 0.002$ the effects of the wind expansion are basically negligible (see Fig. 2 for further comparison),

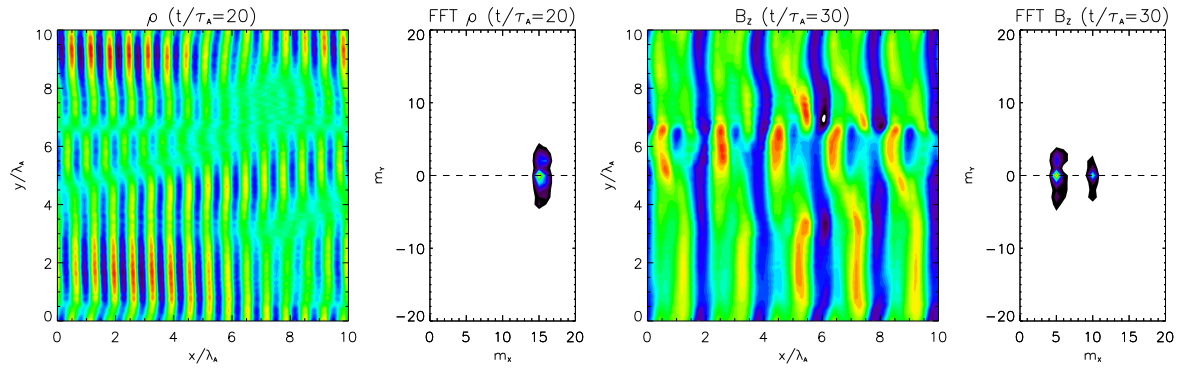

FIGURE 4. 2D plots and spectra of density at $t = 20\,\tau_A$ (left panels) and transverse magnetic component B_z at $t = 30\,\tau_A$ (right panels) for the parallel propagation case with $\epsilon = 0.02$ (`A2-Par`). Quantities are displayed in the comoving frame (without stretching along y). The compressive mode with $m_x = 15$ and the backscattered Alfvénic mode with $m_x = 5$ are clearly visible. The horizontal dashed line in the FFT plots indicates the radial direction of $\mathbf{B_0} \parallel \mathbf{k}_0$.

for $\epsilon = 0.02$ the onset of the instability is slightly delayed and the growth rate is somehow smaller, while for $\epsilon = 0.2$ the effects of the expansion are so strong that the instability is almost suppressed. As predicted, in the latter case of the longest period pump wave, the slow growth of density fluctuations is far from being exponential. Again, this is due to the action of the $\dot{a}/a$ terms in the equations (see the source terms in the original formulation), which are strongly and continuously modifying the background plasma parameters before but even during the onset of the instability. In the bottom panel we show the energy E^+ of the forward propagating Alfvén mode $\mathbf{z}^+$, normalized to its initial value. The expected decay, purely due to the expansion of the medium in which the pump wave propagates, is indicated with dashed lines, for each run. Notice that for the small $\epsilon = 0.002$ value the evolution is almost identical to the non-expanding case. In the intermediate case the expansion affects the evolution, but E^+ drops considerably due to the instability, in spite of the gradual reduction due to the $\dot{a}/a$ terms. For the extreme $\epsilon = 0.2$ (`A3-Par`) case the expansion effects are so strong that no contribution to its decay due to the instability can be seen in the reported range of times. Moreover, we should recall here that quantities have been plotted in terms of time normalized to the pump wave period, so that for increasing ϵ the evolution is actually slower, in absolute terms, also due to the increment of the normalization period τ_A.

Let us now investigate the 2D properties of the decay instability in the presence of wind expansion and consider the intermediate $\epsilon = 0.02$ case (`A2-Par`). In Fig. 4 we plot in the equatorial $x - y$ plane the density ρ at $t = 20\tau_A$, just before the saturation of the instability, and magnetic component B_z at $t = 30\tau_A$, just after saturation, representative of compressive and Alfvénic modes, respectively. Notice that the periodic box has selected a main $m_x = 15$ magneto-acoustic mode along the propagation direction of $\mathbf{k}_0 \parallel \mathbf{B}_0$, though a lower wave number modulation along y is also present. At this time the sound-like waves are about to steepen into a train of shocks, though the mother pump wave is still dominant. As far as the Alfvénic component is concerned, we then need to wait a later time after saturation (occurring around $t = 25\tau_A$, see Fig. 3) to see a dominant daughter wave. We then plot the B_z component at $t = 30\tau_A$, when the $\mathbf{z}^+$ pump wave has basically died and only the backscattered $\mathbf{z}^-$ wave is visible, with $m_x = 5$ and an additional low wave number modulation in the y direction.

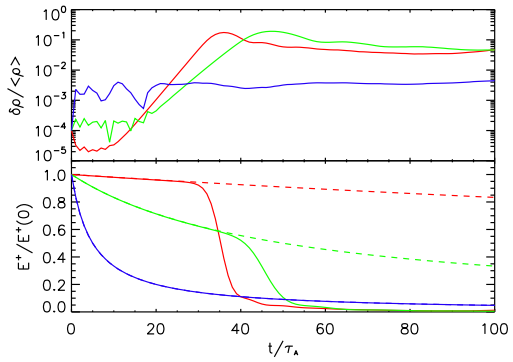

FIGURE 5. Comparison of three simulations with mother wave in oblique propagation. Curves from top to bottom: $\epsilon = 0.002$ (`A1-Obl`, red lines in the color version), $\epsilon = 0.02$ (`A2-Obl`, green), and $\epsilon = 0.2$ (`A3-Obl`, blue). Notations are as in Fig. 3.

The same information can be more easily drawn by investigating the reported 2D spectra, obtained through *Fast Fourier Transforms* (FFT) of the selected physical quantities. The daughter waves are clearly peaked at mode numbers $\mathbf{m} = (15, 0)$ for the compressive component and at $\mathbf{m} = (5, 0)$ for the Alfvénic mode, though *stripes* of excited modes in the y direction are also present at low m_y numbers. We should remind here that parametric decay of pump waves in parallel propagation is essentially a 1D process, so we did not expect to see a large scatter in the 2D spectra. This fact is clearly reflected by the presence of daughter waves that peak in the FFT plots mainly along the dashed line, indicating the radial direction of both $\mathbf{B_0} \parallel \mathbf{k}_0$.

4.2. *Oblique propagation of arc-polarized Alfvén waves*

The situation is quite different in the oblique case. We repeat the same three runs ($\epsilon = 0.002$, $\epsilon = 0.02$, $\epsilon = 0.2$) with Run A parameters, this time with an initial angle $\theta_0 = 30°$ between the pump wave vector $\mathbf{k}_0$ in the radial direction and the background field $\mathbf{B}_0$. The Alfvén wave polarization is now of arc-type, as described in Sect. 3, necessary to preserve an overall $|\mathbf{B}| = \text{const}$ during the evolution and thus to avoid ponderomotive forces that may spoil the development of the decay instability.

In Fig. 5 we plot the comparison of the quantities characterizing the evolution of the instability for the three runs with different expansion factors ϵ, in analogy to the parallel case already shown in Fig. 3. Notice that the overall evolution is now always slower, as shown in Del Zanna (2001), with correspondingly smaller growth rates. We recall that in the oblique case and arc polarization we expect a dependence $\gamma \sim \cos\theta_0$, though for $\theta_0 = 0$ we cannot recover the growth rate for parallel propagation. However, the qualitative behavior of the *rms* quantities is very similar to the case of parallel propagation. The main differences are a somehow stronger decrease of the E^+ energy after saturation, simply due to the later occurrence of the instability, so that the pump wave amplitude is already smaller due to the wind expansion, and a stronger growth of the initial density noise, that completely prevents any sign of instability onset in the extreme expansion case $\epsilon = 0.2$.

The 2D behavior of fluctuations is more interesting in the oblique case. When the decay occurs in 2D two resonance conditions must be satisfied, namely

$$k_{0\parallel} = k_{c\parallel} - k^-_{\parallel}, \quad k_{0\perp} = k_{c\perp} - k^-_{\perp}. \tag{4.3}$$

Since the mother wave propagates along x but the background magnetic field (the parallel

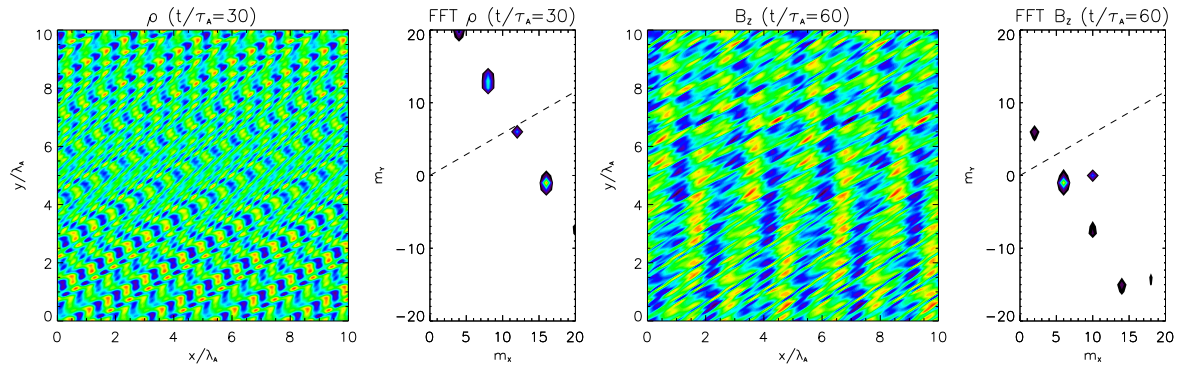

FIGURE 6. 2D plots and spectra of density at $t = 30\,\tau_A$ (left panels) and transverse magnetic component B_z at $t = 60\,\tau_A$ (right panels) for the oblique propagation case `A2-Obl`, in the comoving frame. The dashed line in the FFT plots indicates the initial inclination of $\theta_0 = 30^\circ$ for $\mathbf{B}_0$.

direction) is initially inclined with $\theta = 30^\circ$, $k_{0\perp} \neq 0$ and a direct excitation of transverse modes in the daughter compressive and reflected Alfvénic waves is expected. This is clearly visible in Fig. 6, referring to the intermediate case `A2-Obl`: a compressive mode with a dominant $m_{cx} = 16$ has developed, with fronts no longer aligned along x (the direction of $\mathbf{k}_0$), but roughly along the direction of $\mathbf{B}_0$. A strong modulation is seen in the perpendicular direction too, even at high wave numbers, which was absent in the case of parallel propagation. Similarly, the 2D contours of B_z at $t = 60\tau_A$ (after saturation, when $E^- > E^+$) show the presence of a $m_x^- = 6$ dominant mode, with a mixture of positive and negative m_y^- excited modes and again a strong modulation in the transverse direction too.

The situation is clearer by inspecting the corresponding FFT plots. Since the decay channels are larger in a 2D geometry, allowing more nonlinear interactions, a broadband spectrum of daughter waves is expected. In Fig. 6 we notice that while only a single value of $k_{c\parallel}$ (and $k^-{}_\parallel$) is excited, a range of oblique modes with different $k_{c\perp}$ (and $k_\perp^-$), all sharing the same $k_\parallel$, can be clearly seen in the form of oblique *dotted stripes* in the FFT plots. Here we iterate that the presence of these additional excited waves by mode coupling is due to the fact that $k_{0\perp} \neq 0$ right from the start, then also (at least one of) the daughter waves must have a perpendicular wave vector component.

This 2D behaviour is not peculiar of MHD only, it was actually first observed and discussed in the hybrid regime, for *linearly* polarized oblique waves, where the main difference is that the instability saturation occurs earlier and the mechanism is different (proton trapping). Formation of a proton beam is always observed along $\mathbf{B}_0$, even for oblique propagation, and the electron to proton temperature ratio also plays an important role (Matteini *et al.* 2010*a*; Del Zanna *et al.* 2012*b*).

As far as the effects of expansion are concerned, the situation is that outlined in the sketch of Fig. 7, here in *physical* space, where the lateral stretching in $y \sim a$ and the shrinking in $k_y \sim a^{-1}$ are both taken into account. The inclination of $\mathbf{B}_0$ increases in time (the development of the Parker spiral in the $x-y$ equatorial plane), whereas wave vectors tend towards the (radial) x axis, as k_y decreases. The net result is that any $\mathbf{k}$ which is originally perpendicular to $\mathbf{B}_0$ will always be perpendicular also to the rotated field. On the other hand, the component $\mathbf{k}_\parallel$, initially parallel to $\mathbf{B}_0$ by definition, diverges from that direction as time increases leading to $\mathbf{k}_\parallel \nparallel \mathbf{B}_0$. It is now easy to understand why the

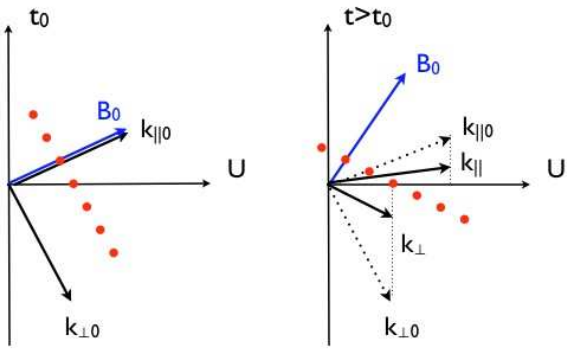

FIGURE 7. Modifications in physical space due to expansion of the background field $\mathbf{B}_0$ and of the wave vector $\mathbf{k}_0$ (the decomposition refers to the field position at time t_0).

stripe of daughter waves always remains perpendicular to $\mathbf{B}_0$: the creation of these modes occurs on a timescale which is much shorter than the expansion, so that the subsequent evolution is only kinematical following the EB stretching, as described just above. If we finally return to Fig. 6, notice that the stripe of transverse modes does not rotate, since its direction is frozen in this *comoving* Fourier space, and this is always perpendicular to the initial $\mathbf{B}_0$ direction. Similar effects are observed in 2D and 3D applications of EB to MHD turbulence evolution studies (Grappin *et al.* 1993; Grappin & Velli 1996; Dong *et al.* 2014).

Notice that here we have shown the results for a moderate value of the expansion factor ($\epsilon = 0.02$), but we would like to stress that the direct excitation of transverse modes is simply a consequence of the oblique propagation of the pump wave in a 2D domain, allowing for extra channels available for decay. Very similar results are obtained with $\epsilon = 0.002$ (or even $\epsilon = 0$), whereas for $\epsilon = 0.2$ the expansion is too strong and prevents the onset of the decay, as shown previously.

4.3. *Non-monochromatic oblique case*

What shown so far refers to the simple case of a monochromatic pump wave. While this is important to investigate the decay instability itself, free from other spurious effects, the model problem is certainly far from being realistic. A superposition of pump Alfvénic modes could be studied, of course, but the problem is that the strength of the magnetic fluctuations do not preserve the condition $|\mathbf{B}| = \text{const}$, so the initial ponderomotive force drives compressive modes that mask those arising from the decay instability that we want to study. A trick to reconcile these two requirements is due to Malara & Velli (1996). While this and subsequent works dealt with 1D parallel propagation and circular polarization, here we apply the method for 2D oblique polarization of arc-type pump waves for the first time. The idea is to preserve the initial settings exactly as described in Sect. 3 for any kind of polarization, with no superposition of individual waves, but to introduce multiple modes by modifying the phase φ. We choose the form

$$\varphi = k_0 x + A \sum_{m=1}^{100} \frac{1}{m} \cos(k_m x + \varphi_m), \tag{4.4}$$

where φ_k is a random phase for each value of $k_m = 2\pi(m/m_0)$ (we recall that $k_0 = 2\pi$) and we set $A = 1$. With this setting the novel $\mathcal{F}(\varphi)$ still provides an arc-polarized Alfvén

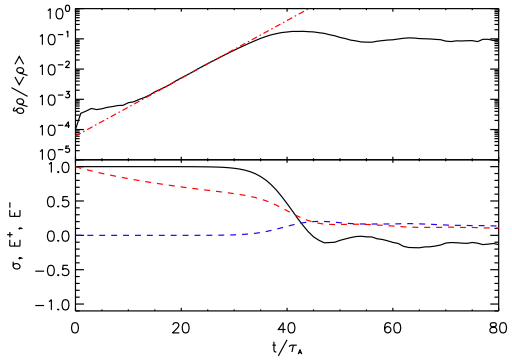

FIGURE 8. The characteristic *rms* quantities for parametric decay for the non-monochromatic case with $\epsilon = 0.02$ (run `nonmon`). The measured instability growth rate is now $\gamma = 0.22$.

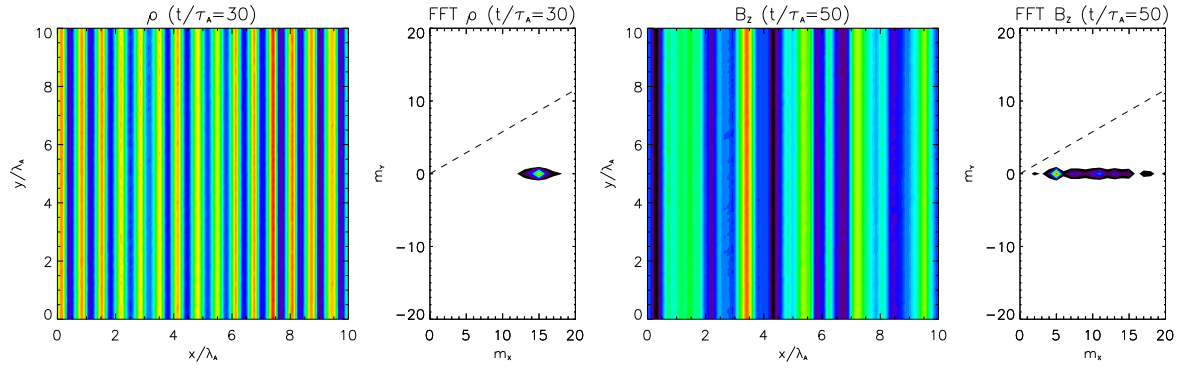

FIGURE 9. 2D plots and spectra of density at $t = 30\,\tau_A$ (left panels) and transverse magnetic component B_z at $t = 50\,\tau_A$ (right panels) for the non-monochromatic case (run `nonmon`).

wave where the mode number $m_0 = 10$ is again the strongest, with tails at both lower and higher values of m, each mode having a power decreasing as m^{-2}.

We repeat the simulation for the most interesting case of $\nu_A = 10^{-3}$ Hz, corresponding to an expansion factor $\epsilon = 0.02$ (we indicate this run as `nonmon`, with the same settings as `A2-Obl` other than the phase φ). In Fig. 8 we show the usual *rms* quantities (normalized density fluctuations, normalized Elsässer energies, and cross helicity) and we can clearly see that the decay instability takes place, though the growth rate is reduced down to $\gamma = 0.22$. The final state is not characterized by a dominance of $\mathbf{z}^-$ modes as in the previous cases with the same parameters, but we see that $E^- \sim E^+$ with oscillations of the cross helicity about $\sigma \sim 0$, though with negative values.

What is somehow unexpected is the 2D behavior of the instability. In Fig. 9 we report, as usual, the 2D plots and spectra of the density fluctuations just before the peak of the instability (left panels) and of the B_z magnetic component right after saturation (right panels). Clearly, no modulation at all is visible in the y direction, in spite of the oblique inclination of the background field of 30° (constant in time in Fourier space, as shown by the dashed lines). On the other hand, the daughter waves are well characterized by $\mathbf{m} = (15, 0)$ for $\delta\rho$ and by $\mathbf{m} = (5, 0)$ for the backscattered Alfvén wave. A larger spread in m_x is observed in the B_z spectrum, due to the presence of the pump wave, which has

not decayed to $E^+ \ll E^-$ values, characterized by a dominant $\mathbf{m} = (10, 0)$ mode with additional components as from Eq. 4.4. The reason for this behavior is that the initial broad-band spectrum of the mother wave imposes much stringent phase relations to be satisfied by the daughter waves as compared to the monochromatic case (Matteini 2012). Resonances are then more difficult to excite perpendicularly to the initial $\mathbf{k}_0$, parallel to the x axis, and the cascade only occurs along that direction, precisely as in a purely 1D case.

5. Conclusions

We presented, for the first time, a detailed analysis of the solar wind expansion effects in two-dimensional MHD simulations of the parametric decay instability of Alfvén waves, for both parallel and oblique propagation. We took advantage of the expanding box (EB) model, here reformulated geometrically by introducing a time-dependent metric tensor $\mathrm{diag}\{1, a^2, a^2\}$, where $a(t)$ is the *Hubble-like* transverse expansion factor. We considered Alfvén waves of low frequency ($\nu \sim 10^{-4} - 10^{-2}$ Hz) as observed in the solar wind, and studied their nonlinear evolution far enough from the Sun, where the solar wind speed U_0 can be considered constant.

The background plasma parameters (namely the fluctuations normalized amplitude $\eta \sim a^{1/2}$ and the plasma $\beta \sim a^{2/3}$) are modified before and during the onset of the instability, typically reducing the expected growth rate, though for extreme values of ϵ the parametric instability may be completely suppressed. For our choice of parameters, appropriate for the inner heliospheric region ($R_0 = 0.25$ AU, $U_0 = 750$ km s^{-1}, $\eta = 0.2$, $\beta = 0.1$), the instability increases very slowly (algebraically) for the mother Alfvén waves with the longest period $\tau_A = 10^4$ s, corresponding to an expansion rate $\epsilon = 0.2$, which is comparable to the growth rate measured in the absence of expansion ($\gamma \simeq 0.63$ for the parallel propagation case). On the other hand, for $\tau_A = 10^3$ s ($\epsilon = 0.02$) there is competition between the mother wave decay due to the expansion and that due to the instability, leading to a 15% reduction of γ but leaving the evolution of quantities in t/τ_A qualitatively unchanged, whereas for $\tau_A = 10^2$ s ($\epsilon = 0.002$) the instability onset and evolution are not substantially affected by the expansion. In the oblique case, with arc-polarized mother waves, the growth rates are always smaller than the corresponding parallel ones.

For a given expansion rate (the intermediate one $\epsilon = 0.02$, corresponding to a frequency $\nu_A = 10^{-3}$ Hz), we investigated the 2D behavior of the compressive and backscattered Alfvénic daughter waves and the spectral properties of such fluctuations. In the parallel case the excited modes lead to $m_c = 15$ and $m^- = 5$ wavelengths in the numerical box along the x direction of $\mathbf{k}_0$ (the pump wave has $m_0 = 10$), with a very little spread in Fourier modes for low m_y transverse modes. The situation changes in the corresponding oblique case. Here we found $m_c = 16$ and $m^- = 6$ along x for the main excited modes, with $m_y = -1$, and other resonant daughter waves are also triggered. Related to the 2D behavior of the parametric decay in the oblique case, two novel results were found in the present work.

First, the stripes of daughter waves seen in Fourier space always form perpendicular to the local $\mathbf{B}_0$, as first observed by Matteini *et al.* (2010*a*) in hybrid simulations (without expansion). When the solar wind expansion is taken into account, this field rotates in time in the equatorial plane by increasing the θ angle with respect to the radial direction, mimicking the presence of the Parker spiral. However, this effect is compensated by the shrinking of the non-radial $\mathbf{k}$ components, thus the stripe of daughter modes, which is created and then remains frozen with the expansion, is always perpendicular to $\mathbf{B}_0$.

Second, if an initial non-monochromatic spectrum is set up for the mother wave (by changing just the phase in order to preserve the condition $|\mathbf{B}_0 + \delta\mathbf{B}| = \text{const}$), the triggering of modes transverse to the local $\mathbf{B}_0$ is no longer found, and all modes are excited along x, with no sign of any modulation along y. This is probably explained by the more stringent requirements for $\mathbf{k}$ and ω that the daughter waves should satisfy for all the excited modes and not just for those arising from the dominant $m_0 = 10$ one. If this result will be confirmed by more general simulations (in full three dimensions and allowing for a spectrum not restricted to the condition of a constant $|\mathbf{B}_0 + \delta\mathbf{B}|$), it would definitely mean that parametric decay is unable to trigger a direct cascade of perpendicular modes, other than just due to purely geometrical effects (at larger distances $\mathbf{k}_0$ and $\mathbf{B}_0$ tend to be progressively more perpendicular).

A final important aspect one should discuss is the possible relation between the decay instability of low-frequency Alfvénic modes and the MHD turbulent cascade, since both features are contemporarily present in the heliospheric plasma. The observations show that the magnetic fluctuations dominate the low-frequency spectrum and are characterized by a ν^{-1} dependence, probably reminiscent of the injection in the solar corona (Verdini *et al.* 2012). At higher frequencies the spectrum is steeper, with the typical Kolmogorov scaling $\nu^{-5/3}$ of fully developed turbulence. The spectral break between the energy-containing scales and the inertial range, however, is seen to depend on the heliocentric distance, and in fast streams this goes roughly as $\nu_\mathrm{b} \simeq 5\times10^{-2}\,\mathrm{Hz}\,(R/0.3\,\mathrm{AU})^{-1.5}$ (e.g. Bruno & Carbone 2013).

We speculate that the solar wind expansion may act as a filter for parametric decay and possibly explain the observed behavior (see also Tenerani & Velli 2013). Waves with $\nu_\mathrm{A} \sim 10^{-2} - 10^{-3}$ Hz, so with periods of minutes, are basically insensitive to the solar wind expansion. Parametric decay is then free to operate by producing $\mathbf{z}^-$ modes out of the initial $\mathbf{z}^+$ ones, thus possibly triggering a turbulent cascade, at least in the original radial direction of the pump wave vector (also parallel to the background field in 1D or oblique to it in 2D). Mother waves with periods of hours, on the other hand, feel the expansion effects, the ϵ parameter is close to the expected parametric decay growth rate, and the instability is strongly delayed or even suppressed. Waves with frequencies of $\nu_\mathrm{A} \sim 10^{-4}$ Hz are thus not expected to evolve, and this seems to be confirmed by the Ulysses observations up to to 4.8 AU, reported also in the cited review, showing that at these frequencies we are still above the spectral break, where the turbulent cascade has not been activated yet. In any case, provided that the simple creation of $\mathbf{z}^-$ radially incoming waves is really enough to trigger the cascade, then the observed decrease of ν_b with R would be naturally explained, as at larger distances (longer times), smaller and smaller frequency modes are expected to become parametrically unstable.

These aspects obviously would require a deeper understanding and a quantitative comparison with real data, as well as the possible relation between parametric decay of oblique waves and the transverse turbulent cascade should be studied carefully in detail. However, we deem that these subjects are beyond the goal of the present paper, and we leave more quantitative estimations and further discussions as future work.

The authors thank Roland Grappin for stimulating discussions and two anonymous referees for their useful suggestions. The research leading to these results has received funding from the European Commission's Seventh Framework Program (FP7/2007-2013) under the grant agreement SHOCK (project number 284515). The research described in this paper was also supported by the UK Science and Technology Facilities Council grant ST/K001051/1, and by a grant from the Interuniversity Attraction Poles Programme initiated by the Belgian Science Policy Office (IAP P7/08 CHARM). This work was

carried out in part at the Jet Propulsion Laboratory under a contract with NASA. We also acknowledge support from the Italian Space Agency.

REFERENCES

Araneda, J. A., Marsch, E. & F.-Viñas, A. 2008 Proton Core Heating and Beam Formation via Parametrically Unstable Alfvén-Cyclotron Waves. *Physical Review Letters* **100** (12), 125003.

Barnes, A. & Hollweg, J. V. 1974 Large-amplitude hydromagnetic waves. *J. Geophys. Res.* **79**, 2302.

Bavassano, B., Pietropaolo, E. & Bruno, R. 2000 On the evolution of outward and inward Alfvénic fluctuations in the polar wind. *J. Geophys. Res.* **105**, 15959–15964.

Belcher, J. W. & Davis, Jr., L. 1971 Large-amplitude Alfvén waves in the interplanetary medium, 2. *J. Geophys. Res.* **76**, 3534.

Breech, B., Matthaeus, W. H., Minnie, J., Oughton, S., Parhi, S., Bieber, J. W. & Bavassano, B. 2005 Radial evolution of cross helicity in high-latitude solar wind. *Geophys. Res. Lett.* **32**, 6103.

Bruno, R., Bavassano, B. & Villante, U. 1985 Evidence for long period Alfven waves in the inner solar system. *J. Geophys. Res.* **90**, 4373–4377.

Bruno, R. & Carbone, V. 2013 The Solar Wind as a Turbulence Laboratory. *Living Reviews in Solar Physics* **10**, 2.

Del Zanna, L. 2001 Parametric decay of oblique arc-polarized Alfvén waves. *Geophys. Res. Lett.* **28**, 2585–+.

Del Zanna, L. 2009 The ECHO Code for Classical and Relativistic MHD. In *Numerical Modeling of Space Plasma Flows: ASTRONUM-2008* (ed. N. V. Pogorelov, E. Audit, P. Colella & G. P. Zank), *Astronomical Society of the Pacific Conference Series*, vol. 406, p. 217.

Del Zanna, L., Landi, S., Matteini, L. & Velli, M. 2012*a* The Expanding Box Model in ECHO: Application to the Parametric Decay of Alfvén Waves in the Fast Solar Wind. In *Numerical Modeling of Space Plasma Slows (ASTRONUM 2011)* (ed. N. V. Pogorelov, J. A. Font, E. Audit & G. P. Zank), *Astronomical Society of the Pacific Conference Series*, vol. 459, p. 196.

Del Zanna, L., Matteini, L., Landi, S. & Velli, M. 2012*b* Parametric decay of large-amplitude Alfvén waves: MHD and hybrid simulations. In *American Institute of Physics Conference Series* (ed. J. Heerikhuisen, G. Li, N. Pogorelov & G. Zank), *American Institute of Physics Conference Series*, vol. 1436, pp. 12–17.

Del Zanna, L. & Velli, M. 2002 Coronal heating through Alfven waves. *Advances in Space Research* **30**, 471–480.

Del Zanna, L., Velli, M. & Londrillo, P. 2001 Parametric decay of circularly polarized Alfvén waves: Multidimensional simulations in periodic and open domains. *A&A* **367**, 705–718.

Del Zanna, L., Zanotti, O., Bucciantini, N. & Londrillo, P. 2007 ECHO: a Eulerian conservative high-order scheme for general relativistic magnetohydrodynamics and magnetodynamics. *A&A* **473**, 11–30.

Derby, Jr., N. F. 1978 Modulational instability of finite-amplitude, circularly polarized Alfven waves. *ApJ* **224**, 1013–1016.

Dobrowolny, M., Mangeney, A. & Veltri, P. 1980 Fully developed anisotropic hydromagnetic turbulence in interplanetary space. *Physical Review Letters* **45**, 144–147.

Dong, Y., Verdini, A. & Grappin, R. 2014 Evolution of turbulence in the expanding solar wind: a numerical stuty. *ApJ* **submitted**.

Galeev, A. A. & Oraevskii, V. N. 1963 The Stability of Alfvén Waves. *Soviet Physics Doklady* **7**, 988.

Ghosh, S., Vinas, A. F. & Goldstein, M. L. 1993 Parametric instabilities of a large-amplitude circularly polarized Alfven wave - Linear growth in two-dimensional geometries. *J. Geophys. Res.* **98**, 15561.

Goldstein, M. L. 1978 An instability of finite amplitude circularly polarized Alfven waves. *ApJ* **219**, 700–704.

Goldstein, M. L., Roberts, D. A. & Matthaeus, W. H. 1995 Magnetohydrodynamic Turbulence In The Solar Wind. *ARA&A* **33**, 283–326.

Grappin, R., Mangeney, A. & Marsch, E. 1990 On the origin of solar wind MHD turbulence - HELIOS data revisited. *J. Geophys. Res.* **95**, 8197–8209.

Grappin, R. & Velli, M. 1996 Waves and streams in the expanding solar wind. *J. Geophys. Res.* **101**, 425–444.

Grappin, R., Velli, M. & Mangeney, A. 1993 Nonlinear wave evolution in the expanding solar wind. *Physical Review Letters* **70**, 2190–2193.

Hellinger, P., Velli, M., TráVníČEk, P., Gary, S. P., Goldstein, B. E. & Liewer, P. C. 2005 Alfvén wave heating of heavy ions in the expanding solar wind: Hybrid simulations. *Journal of Geophysical Research (Space Physics)* **110**, 12109.

Hollweg, J. V. 1994 Beat, modulational, and decay instabilities of a circularly polarized Alfven wave. *J. Geophys. Res.* **99**, 23431.

Horbury, T. S., Forman, M. A. & Oughton, S. 2005 Spacecraft observations of solar wind turbulence: an overview. *Plasma Physics and Controlled Fusion* **47**, B703–B717.

Hoshino, M. & Goldstein, M. L. 1989 Time evolution from linear to nonlinear stages in magnetohydrodynamic parametric instabilities. *Physics of Fluids B* **1**, 1405–1415.

Inhester, B. 1990 A drift-kinetic treatment of the parametric decay of large-amplitude Alfven waves. *J. Geophys. Res.* **95**, 10525–10539.

Landi, S., Londrillo, P., Velli, M. & Bettarini, L. 2008 Three-dimensional simulations of compressible tearing instability. *Physics of Plasmas* **15** (1), 012302–+.

Liewer, P. C., Velli, M. & Goldstein, B. E. 2001 Alfvén wave propagation and ion cyclotron interactions in the expanding solar wind: One-dimensional hybrid simulations. *J. Geophys. Res.* **106**, 29261–29282.

Lionello, R., Velli, M., Downs, C., Linker, J. A., Mikić, Z. & Verdini, A. 2014 Validating a Time-dependent Turbulence-driven Model of the Solar Wind. *ApJ* **784**, 120.

Londrillo, P. & Del Zanna, L. 2004 On the divergence-free condition in Godunov-type schemes for ideal magnetohydrodynamics: the upwind constrained transport method. *J. Comput. Phys.* **195**, 17–48.

Malara, F., Primavera, L. & Veltri, P. 2000 Nonlinear evolution of parametric instability of a large-amplitude nonmonochromatic Alfvén wave. *Physics of Plasmas* **7**, 2866–2877.

Malara, F. & Velli, M. 1996 Parametric instability of a large-amplitude nonmonochromatic Alfvén wave. *Physics of Plasmas* **3**, 4427–4433.

Marsch, E. & Tu, C.-Y. 1990 On the radial evolution of MHD turbulence in the inner heliosphere. *J. Geophys. Res.* **95**, 8211–8229.

Matteini, L. 2012 Parametric decay of Alfvén waves at parallel and oblique propagation: Kinetic effects and transverse couplings. In *American Institute of Physics Conference Series* (ed. P.-L. Sulem & M. Mond), *American Institute of Physics Conference Series*, vol. 1439, pp. 83–93.

Matteini, L., Horbury, T. S., Neugebauer, M. & Goldstein, B. E. 2014 Dependence of solar wind speed on the local magnetic field orientation: Role of Alfvénic fluctuations. *Geophys. Res. Lett.* **41**, 259–265.

Matteini, L., Landi, S., Del Zanna, L., Velli, M. & Hellinger, P. 2010*a* Parametric decay of linearly polarized shear Alfvén waves in oblique propagation: One and two-dimensional hybrid simulations. *Geophys. Res. Lett.* **37**, 20101.

Matteini, L., Landi, S., Hellinger, P. & Velli, M. 2006 Parallel proton fire hose instability in the expanding solar wind: Hybrid simulations. *Journal of Geophysical Research (Space Physics)* **111**, 10101.

Matteini, L., Landi, S., Velli, M. & Hellinger, P. 2010*b* Kinetics of parametric instabilities of Alfvén waves: Evolution of ion distribution functions. *Journal of Geophysical Research (Space Physics)* **115**, 9106.

Nariyuki, Y. & Hada, T. 2006 Kinetically modified parametric instabilities of circularly polarized Alfvén waves: Ion kinetic effects. *Physics of Plasmas* **13** (12), 124501.

Nariyuki, Y., Hada, T. & Tsubouchi, K. 2007 Parametric instabilities of parallel propagating incoherent Alfvén waves in a finite ion beta plasma. *Physics of Plasmas* **14** (12), 122110.

Riley, P., Sonett, C. P., Tsurutani, B. T., Balogh, A., Forsyth, R. J. & Hoogeveen,

G. W. 1996 Properties of arc-polarized Alfvén waves in the ecliptic plane: Ulysses observations. *J. Geophys. Res.* **101**, 19987–19994.

Roberts, D. A., Goldstein, M. L., Klein, L. W. & Matthaeus, W. H. 1987 Origin and evolution of fluctuations in the solar wind - HELIOS observations and Helios-Voyager comparisons. *J. Geophys. Res.* **92**, 12023–12035.

Sagdeev, R. Z. & Galeev, A. A. 1969 *Nonlinear Plasma Theory*. Benjamin, New York.

Tenerani, A. & Velli, M. 2013 Parametric decay of radial Alfvén waves in the expanding accelerating solar wind. *Journal of Geophysical Research (Space Physics)* **118**, 7507–7516.

Tsurutani, B. T. & Ho, C. M. 1999 A review of discontinuities and Alfvén waves in interplanetary space: Ulysses results. *Reviews of Geophysics* **37**, 517–524.

Tu, C.-Y. & Marsch, E. 1990 Evidence for a 'background' spectrum of solar wind turbulence in the inner heliosphere. *J. Geophys. Res.* **95**, 4337–4341.

Umeki, H. & Terasawa, T. 1992 Decay instability of incoherent Alfven waves in the solar wind. *J. Geophys. Res.* **97**, 3113–3119.

Vasquez, B. J. & Hollweg, J. V. 1996 Formation of arc-shaped Alfvén waves and rotational discontinuities from oblique linearly polarized wave trains. *J. Geophys. Res.* **101**, 13527–13540.

Velli, M., Grappin, R. & Mangeney, A. 1992 MHD turbulence in an expanding atmosphere. In *Electromechanical Coupling of the Solar Atmosphere* (ed. D. S. Spicer & P. MacNeice), *American Institute of Physics Conference Series*, vol. 267, pp. 154–159.

Verdini, A., Grappin, R., Pinto, R. & Velli, M. 2012 On the Origin of the 1/f Spectrum in the Solar Wind Magnetic Field. *ApJLett* **750**, L33.

Verdini, A. & Velli, M. 2007 Alfvén Waves and Turbulence in the Solar Atmosphere and Solar Wind. *ApJ* **662**, 669–676.

Verdini, A., Velli, M., Matthaeus, W. H., Oughton, S. & Dmitruk, P. 2010 A Turbulence-Driven Model for Heating and Acceleration of the Fast Wind in Coronal Holes. *ApJLett* **708**, L116–L120.

Viñas, A. F. & Goldstein, M. L. 1991 Parametric instabilities of circularly polarized large-amplitude dispersive Alfvén waves: excitation of parallel-propagating electromagnetic daughter waves. *Journal of Plasma Physics* **46**, 107.